Journal of Physics: Conference Series

PAPER • **OPEN ACCESS**

Solar neutrino results and future prospects with the Borexino detector

To cite this article: L. Miramonti *et al* 2021 *J. Phys.: Conf. Ser.* **1766** 012006

View the article online for updates and enhancements.

IOP ebooks™

Bringing together innovative digital publishing with leading authors from the global scientific community.

Start exploring the collection–download the first chapter of every title for free.

This content was downloaded from IP address 146.241.150.0 on 25/02/2021 at 12:30

Solar neutrino results and future prospects with the Borexino detector

L. Miramonti[1] for the Borexino Collaboration:[2]

M. Agostini, K. Altenmüller, S. Appel, V. Atroshchenko, Z. Bagdasarian, D. Basilico, G. Bellini, J. Benziger, D. Bick, G. Bonfini, D. Bravo, B. Caccianiga, F. Calaprice, A. Caminata, L. Cappelli, P. Cavalcante, F. Cavanna, A. Chepurnov, K. Choi, D. D'Angelo, S. Davini, A. Derbin, A. Di Giacinto, V. Di Marcello, X.F. Ding, A. Di Ludovico, L. Di Noto, I. Drachnev, A. Formozov, D. Franco, F. Gabriele, C. Galbiati, M. Gschwender, C. Ghiano, M. Giammarchi, A. Goretti, M. Gromov, D. Guffanti, C. Hagner, E. Hungerford, Aldo Ianni, Andrea Ianni, A. Jany, D. Jeschke, S. Kumaran, V. Kobychev, G. Korga, T. Lachenmaier, M. Laubenstein, E. Litvinovich, P. Lombardi, I. Lomskaya, L. Ludhova, G. Lukyanchenko, L. Lukyanchenko, I. Machulin, G. Manuzio, S. Marcocci, J. Maricic, J. Martyn, E. Meroni, M. Meyer, L.Miramonti, M. Misiaszek, V. Muratova, B. Neumair, M. Nieslony, L. Oberauer, V. Orekhov, F. Ortica, M. Pallavicini, L. Papp, O. Penek, L. Pietrofaccia, N. Pilipenko, A. Pocar, G. Raikov, M.T. Ranalli, G. Ranucci, A. Razeto, A. Re, M. Redchuk, A. Romani, N. Rossi, S. Rottenanger, S. Schönert, D. Semenov, M. Skorokhvatov, O. Smirnov, A. Sotnikov, Y. Suvorov, R. Tartaglia, G. Testera, J. Thurn, E. Unzhakov, A. Vishneva, R.B. Vogelaar, F. von Feilitzsch, M. Wojcik, M. Wurm, O. Zaimidoroga, S. Zavatarelli, K. Zuber, G. Zuzel

[1] Dipartimento di Fisica dell'Università di Milano and INFN
Via Celoria 16, I 20133 Milano, Italy

E-mail: lino.miramonti@mi.infn.it

Abstract. Neutrinos coming from the Sun have played a crucial role in the discovery of neutrino oscillations and they still are proving to be a unique and powerful tool in the investigation of the fusion reactions that power the stars, as well as representing a probe to study the basic neutrino properties. The Borexino detector has started its data acquisition in 2007 in the underground Gran Sasso National Laboratories (LNGS) in Italy. The main goal of Borexino is the real-time study of low energy neutrinos with an energy threshold as low as about 50 keV. A first phase named Borexino Phase-I started in 2007 and ended in 2010, then after a purification campaign, data-taking resumed in 2011 with the so-called Borexino Phase-II. I will present the recent results of Borexino for the measurement of the four main solar neutrino

[2]

E-mail: spokeperson-borex@lngs.infn.it

Content from this work may be used under the terms of the Creative Commons Attribution 3.0 licence. Any further distribution of this work must maintain attribution to the author(s) and the title of the work, journal citation and DOI.
Published under licence by IOP Publishing Ltd

components of the *pp* fusion chain (*pp*, *pep*, ^{7}Be, ^{8}B), and the upper limits on the remaining two solar neutrino fluxes (CNO and *hep*).

1. Solar neutrinos production and neutrino fluxes

Electron neutrinos (ν_e) are copiously produced by thermonuclear reactions that occur in the core of the stars where protons fuse producing helium, nuclei and energy. Solar neutrinos emitted by the Sun provide a direct and unique tool to study the properties of the interior of our star. In stars protons fuse in reactions within the *pp* chain. Concerning the CNO cycle, the more massive the star is, the more important is this cycle's contribution. In the Sun, the *pp* chain accounts for about 99%, while the remaining percentage is due to the CNO cycle [1, 2]. In the middle of 1960s John Bahcall developed a model of the Sun, the Standard Solar Model (SSM), with the aim to accurately reproduce the physical characteristics of the Sun, in terms of the spectrum and fluxes of the neutrino components produced therein [3].

Figure 1 and Figure 2 respectively show the *pp* chain, with the relative branching percentages, and the CNO cycle – while Figure 3 shows the corresponding predicted neutrino fluxes.

At low energies, the spectrum is dominated by ν_es coming from the primary proton-proton reaction and the spectrum extends up to about 18.8 MeV by neutrinos created in the proton capture of ^{3}He. At high energy the spectrum is dominated by neutrino emitted in the β^+ decay of ^{8}B.

Beside the continuous spectra there are two mono-energetic lines from the electron capture on ^{7}Be ($E_\nu = 0.384$ MeV with a BR of ∼10% and 0.862 MeV with a BR of ∼90%) and one mono-energetic line from the proton-electron-proton fusion ($E_\nu = 1.44$ MeV). Solar ν_es are labeled according to the reaction in which they are produced i.e. *pp*, *hep*, ^8B, ^7Be and *pep* ν_es.

The energy spectrum of neutrinos from the CNO cycle is the result of three continuous spectra with end point energies of 1.19 MeV (^{13}N), 1.73 MeV (^{15}O) and 1.74 MeV (^{17}F). Solar neutrinos emitted by the CNO cycle have never been directly measured and with current technologies it it practically impossible to disentangle the three contributions. These solar neutrinos are labeled *CNO* ν_es.

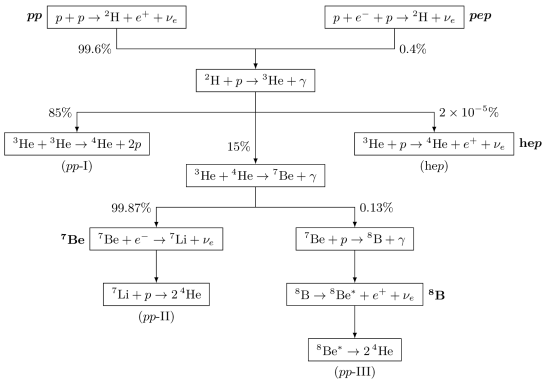

Figure 1. The *pp* chain (ppI, ppII, ppIII), with branching percentages indicated.

2. Helioseismology and Solar Metallicity Problem

Helioseismology is the science that studies the natural oscillations of the Sun, providing a perfect tool to determine the structure of the solar interior. In the '90s there was a rapid development

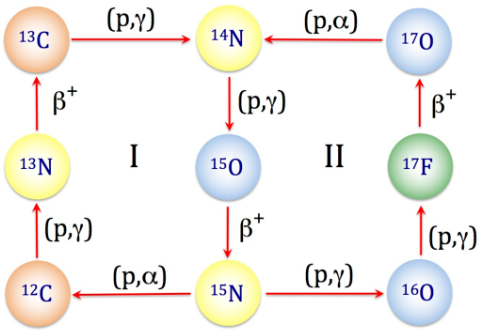

Figure 2. The CNO cycle. The CN cycle, marked I, produces ∼1% of solar energy and significant fluxes of solar neutrinos.

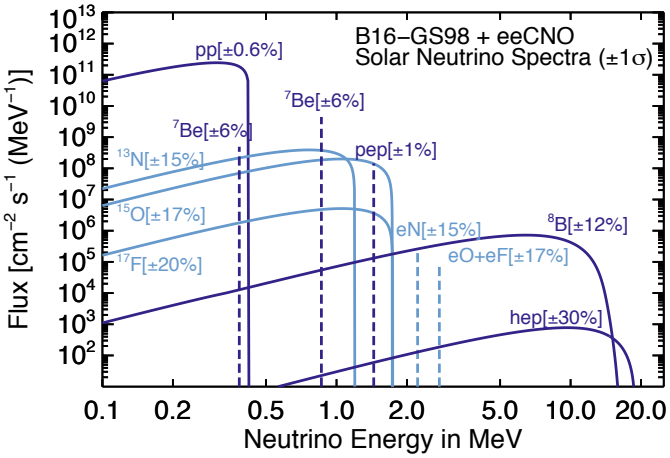

Figure 3. Predicted neutrino fluxes from the Standard Solar Model.

of helioseismic observations and analysis techniques, which led to an accurate characterization of the solar interior.

Recently, the previously excellent agreement between helioseismology measurements and the SSM has been compromised due to a downward revision of the heavy element content at the solar surface; from (Z/X) = 0.0229 [5] to (Z/X) = 0.0165 [6].[3]

[3] All elements hevier than helium are called metals and their total abundance by mass is denoted by Z, while

Table 1. Solar neutrino fluxes foreseen for the LZ-SSM and the HZ-SSM (see text). Units are: 10^{10} (pp), 10^9 (^{7}Be), 10^8 (pep, ^{13}N, ^{15}O), 10^6 (^{8}B,^{17} F) and 10^3(hep) cm^{-2}s^{-1}. Table adopted from [4].

Flux	**B16-GS98**	**B16-AGSS09met**
$\phi(pp)$	5.98 (1 ± 0.006)	6.03 (1 ± 0.005)
$\phi(pep)$	1.44 (1 ± 0.01)	1.46 (1 ± 0.009)
$\phi(hep)$	7.98 (1 ± 0.30)	8.25 (1 ± 0.30)
$\phi(^7Be)$	4.93 (1 ± 0.06)	4.50 (1 ± 0.06)
$\phi(^8B)$	5.46 (1 ± 0.12)	4.50 (1 ± 0.12)
$\phi(^{13}N)$	2.78 (1 ± 0.15)	2.04 (1 ± 0.14)
$\phi(^{15}O)$	2.05 (1 ± 0.17)	1.44 (1 ± 0.16)
$\phi(^{17}F)$	5.29 (1 ± 0.20)	3.26 (1 ± 0.18)

This discrepancy is known as Solar Metallicity Problem (SMP) (see Figure 4). This problem could be solved either by revisiting the physical inputs of the SSM or modifying the core abundances, in particular those of carbon, nitrogen and oxygen. In 2009, with a 3-D hydrodynamical model, a new revision of the abundances of almost all elements in the solar photosphere has been done [7]. This new result gave a solar abundance (Z/X) = 0.0178.

This three sets of solar abundances (GS98 [5], AGS05 [6], AGSS09 [7]) have been used in [8] giving rise to two different SSMs named the Low-Metallicity (LZ) SSM and the High-Metallicity (HZ) SSM. See also [9] and [10].

A possible way to disentangle the LZ-SSM from the HZ-SSM is to measure the ^{7}Be, ^{8}B or CNO neutrino fluxes, which are sensitive to the solar metallicity content.

Table 1 reports the neutrino fluxes expected from the SSM in the case of LZ-SSM and HZ-SSM [4]. As it can be deduced the difference between the two metallicities is about 9% for ^{7}Be ν_e, about 18% for ^{8}B ν_e and almost 40% for CNO ν_e.

3. Neutrino flavor conversion in vacuum and matter

The flavor conversion of solar neutrinos is described by simple expressions; the survival probability is computed numerically to correctly include the number density of scatterers along the trajectory of neutrinos from the production site to where they will be detected.

For the flavor conversion of solar neutrino, ν_μ and ν_τ are indistinguishable and therefore the survival probability of ν_e is the only function that we need in order to describe the flavor composition of the solar neutrino flux. The solar neutrino survival probability depends on the solar oscillation parameters θ_{12}, Δm^2_{21} and θ_{13}.

For low energy neutrinos the flavor change occurs in vacuum while for high energy neutrinos flavor change is dominated by matter oscillations (which adjust the previous expression by the addition of an effective matter potential in the Hamiltonian, effectively shifting the ν_e mass upward, through the Mikheev-Smirnov-Wolfenstein (MSW) effect). The transition regime between vacuum oscillations and matter driven oscillations is at about some MeV. For a review on solar neutrino flavor conversion in vacuum and matter see [11].

the hydrogen abundance by mass is denoted by X.

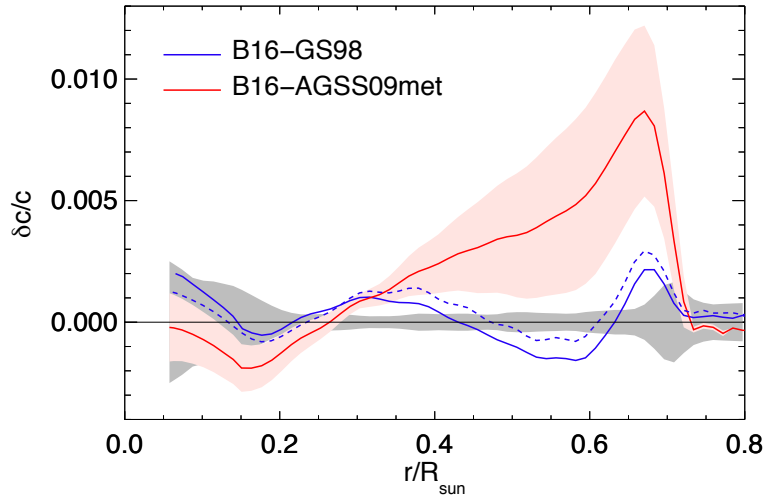

Figure 4. Fractional sound speed difference; in blue the high metallicity and in red the low metallicity. Figure from [4].

4. Solar Neutrinos Detection

There are two techniques used to detect solar neutrinos. A first one take advantage of radiochemical (counting) methods; using isotopes which, once having interacted with an electron neutrino, produce radioactive isotopes whose decay signature can be detected:

$$\nu_e + {}^{A}_{Z}X \rightarrow {}^{A}_{Z+1}Y + e^- \tag{1}$$

A second method is based on elastic scattering of the neutrino off electrons:

$$\nu_x + e^- \rightarrow \nu_x + e^- \tag{2}$$

In real time experiments, all neutrino types undergo this reaction, but for ν_μ and ν_τ the cross section is about six times smaller than ν_e at the relevant energies, since it is mediated only by neutral current (NC) interactions, while for ν_e charged currents (CC) are also at play.

5. From Homestake to SNO

The first solar neutrino experiment operated continuously from 1970 until 1994 in the Homestake gold mine in South Dakota [12]. A large tank containing 615 tonnes of liquid perchloroethylene was exposed to solar neutrinos looking for the reaction $\nu_e + {}^{37}Cl \rightarrow {}^{37}Ar + e^-$. Being the energy threshold of this reaction $E_{th} = 814\,keV$, only ^{7}Be and ^{8}B neutrinos were detected. The number of detected neutrinos was only about 1/3 compared to that expected from the SSM, giving rise to what was dubbed as the Solar Neutrino Problem (SNP).

At the beginning of the 1980s, in the Kamioka mine in Japan, the first real time solar neutrino detector was built. The KamiokaNDE detector [13] consisted of a large water Čerenkov detector with a total mass of 3000 tonnes of pure water instrumented with 1000 PMTs. The energy threshold of the reaction was about $E_{th} = 7.5\ MeV$ allowing only the detectction of ^{8}B and *hep* neutrinos. At the beginning of the '90s a much bigger detector was realized. The Super-Kamiokande detector, still in operation, consists of an active mass of 50,000 tonnes of pure water instrumented with 11200 PMTs. The energy threshold was lowered to about $E_{th} = 5.5\ MeV$ [14]. The number of neutrinos detected with both detectors was about 1/2 lower than expected by the SSM, strengthening the case for the real existence of the Solar Neutrino Problem.

In 1990, in order to detect *pp* neutrinos –whose flux is less model-dependent and hence more robust to prove the validity of the SSM– two radiochemical experiments, both employing the reaction $\nu_e + {}^{71}Ga \rightarrow {}^{71}Ge + e^-$, were built. The energy threshold of this reaction is $E_{th} = 233\ keV$. The Gallex experiment was located at the Gran Sasso underground laboratory in Italy and employed 30 tonnes of natural gallium [15] [16], while the Soviet-American experiment SAGE was located in the Baksan underground laboratory and employed 50 tonnes of metallic gallium [17]. The neutrino signal detected both by Gallex and SAGE was smaller than the one predicted by the SSM by about 60%.

In May 1999 a new solar neutrino detector came into play. The Sudbury Neutrino Observatory (SNO) located in Creighton Mine in Sudbury, Canada. It consisted of 1000 tonnes of heavy water viewed by 9600 PMTs allowing to detect neutrinos interacting through both charged currents (CC) and neutral currents (NC) independently [18]. In the CC interaction, the impinging neutrino converts the neutron of the deuteron to a proton $\nu_e + d \rightarrow p + p + e^-$. This reaction is possible only for electron neutrinos, as introduced in the previous subsection. In the NC interaction, the neutrino dissociates the deuteron, breaking it into its constituent neutron and proton $\nu_x + d \rightarrow p + n + \nu_x$. This reaction is possible for all neutrino flavor types. The ϕ_{CC} flux is given only from ϕ_{ν_e} while the ϕ_{NC} flux is given by all neutrino types $\phi_{\nu_e}, \phi_{\nu_\mu}, \phi_{\nu_\tau}$, as mentioned above. While the measured flux via ϕ_{CC} is about 1/3 compared with was expected from theory the measured flux via ϕ_{NC} reaction is comparable with the one expected from the SSM, confirming that actually ν_e are converted into ν_μ and ν_τ during their travel from the core of the Sun to Earth and therefore solving the SNP.

6. Borexino

The Borexino detector is located at the Gran Sasso National Laboratories (LNGS) in central Italy, at a minimum overburden of $\sim$ 1.4 km of rock, equivalent to 3800 m of water. The flux of cosmic muons which cross the rock shielding and reach the underground halls is $\sim$ 1.2 μ $m^{-2}h^{-1}$. Fig. 5 shows a 3D sketch of the detector [19].

The active mass is composed of 278 tonnes of pseudocumene doped with 1.5 g/l of PPO wavelength shifter in order to enhance the scintillator properties with respect to the instrumentation's sensitivity, and it is contained in an 8.5m-diameter nylon Inner Vessel with a thickness of 125 μm. The Inner Vessel is surrounded by two concentric pseudocumene buffers doped with a light-emission quencher (DMP). A Stainless Steel Sphere with a diameter of 13.7 m contains the scintillator and buffers. In turn this sphere is enclosed in a Water Tank, in the shape of a dome, containing 2100 tonnes of ultra-pure water as an additional shield.

The light created by the scintillator is detected by 2212 8" PhotoMultiplier Tubes (PMTs) distributed on the inner surface of the Stainless Steel Sphere. Into the Water Tank, 208 8" PMTs detect the Čerenkov light radiated by cosmic muons. The principle of neutrino detection is based on elastic scattering on electrons in the target material, as introduced in the previous section.

The light yield of the scintillator is $\sim 10^4$ photons per MeV, corresponding to $\sim$500 detected photoelectrons per MeV.

The fast time response of $\sim$3 ns allows for the reconstruction of the event's position by means of a time-of-flight technique; the accuracy in position reconstruction is within $\sim$13 cm. Thanks to this position reconstruction it is possible to define a fiducial volume between 75 tonnes and 150 tonnes depending on the analysis type.

The light created in the fluor molecule by the emission of the scattered electron is emitted isotropically; thus it is impossible to distinguish the light from the signal from the one produced by β and γ rays emitted by radioactive isotopes. In order to reach a signal-to-noise ratio on the order of one, the ^{238}U and ^{232}Th content must be reduced to the level of $10^{-16} g(U)/g$ corresponding to about one count per day (cpd) per 100 tonnes.

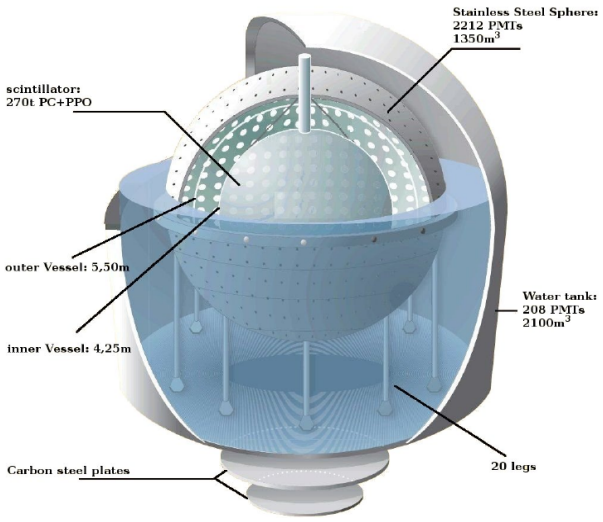

Figure 5. Sketch of the Borexino detector. The base of the dome-like structure is 18 m in diameter.

Several techniques have been applied in order to reduce the radioisotope content in the scintillator – such as distillation, water extraction and nitrogen stripping [20] and [21].

7. First Simultaneous Precision Spectroscopy of pp, ^{7}Be, and pep

Borexino began to take data in 2007. In 2010 started an extensive purification campaign consisting of six cycles of closed-loop water extraction that continued for about two years.

In 2012 Borexino resumed taking data with a new phase, namely *PhaseII*. The radioactive contaminants were significantly reduced; ^{238}U and ^{232}Th were reduced at a level of $< 9.4 \times 10^{-20}$ g/g (95% C.L.) and $< 5.7 \times 10^{-19}$ g/g (95% C.L.) respectively while ^{85}Kr was reduced by a factor of about 5 and ^{210}Bi by a factor of about 2.

Exploiting the number of detected photons and their detection times it is possible to reconstruct, for each event, the energy, the position and the pulse shape. The energy resolution is ~ 50 keV at 1 MeV while the hardware energy threshold is $N_p > 20$, corresponding to $\sim$50 keV.

To suppress cosmogenic backgrounds, events are selected removing internal muons and applying a 300 ms veto (2 ms for external muons), the total dead-time introduced by these vetos in about 1.5%.

The fast coincidences of ^{214}Bi -^{214}Po within the ^{238}U chain and unphysical noise events can be removed with a fractional loss of good events that is $\sim 0.1\%$ [22].

In order to reduce the background coming from external sources such as the nylon vessel, the SSS and the PMTs, a Fiducial Volume (FV) cut is software-defined. The FV for most solar neutrino analyses roughly consists of a cut on the radius $R < 2.8$ m and a cut on the vertical coordinate $-1.8 < z < 2.2$ m; in this way only the innermost region of the scintillator is selected corresponding to 71.3 t of liquid scintillator.

The main background that remains in the fiducial volume after all these cuts comes from the radioactive isotopes contained in the liquid scintillator: the ^{14}C which β^-decay (Q = 156 keV), the α decay of ^{210}Po (E = 5.3 MeV quenched by a factor $\sim$10), the ^{85}Kr which β^- decays (Q = 687 keV), and the ^{210}Bi which β^- decays (Q = 1160 keV).

Another important background, in particular for the *pp* ν analysis is due to the pile-up of uncorrelated events coming from ^{14}C, external background, and ^{210}Po [22].

Besides, residual external background comes from γ rays emitted by ^{208}Tl, ^{214}Bi, and ^{40}K decays.

The cosmogenic isotope ^{11}C (β^+ decay, $\tau = 29.4\,\mathrm{min}$) is continuously produced by muons crossing the detector through spallation reactions on ^{12}C. In order to suppress this cosmogenic isotope, the Borexino Collaboration has developed a method based on a Three-Fold Coincidence (TFC). It it possible to tag events correlated in space and time with a muon and a neutron, and in order to better disentangle the ^{11}C events, a e^+/e^- pulse-shape discrimination is also applied [23, 24]. The ^{11}C-tagging efficiency of the TFC algorithm is $(92 \pm 4)\%$.

The strategy to separate the solar ν signals from the radioactive background is based on maximizing a binned likelihood function, through a multivariate approach, built as the product of four factors which are: (i) the TFC-subtracted spectrum, (ii) the TFC-tagged energy spectrum, (iii) the pulse shape discrimination parameter PS-$\mathcal{L}_{\mathrm{PR}}$ (defined as the maximum value of the likelihood function $\mathcal{L}_{\mathrm{PR}}$ used in the position reconstruction, divided by the value of the energy estimator), and (iv) the radial distribution of the events.

Two different approaches have been adopted by the Borexino Collaboration to fit the data. A first approach is based on the analytical description of the detector response function and a second one is fully based on MonteCarlo (MC) simulations.

In order to obtain the interaction rates of *pp*, ^{7}Be, and *pep* neutrinos the energy spectrum has been fitted together with the decay rates of ^{85}Kr, ^{210}Po, ^{210}Bi, ^{11}C, and the external backgrounds due to γ rays emitted by ^{208}Tl, ^{214}Bi, and ^{40}K.

The interaction rate of CNO νs has been constrained to the value of the HZ-SSM predictions, including MSW-LMA (Large Mixing Angle) oscillations to $4.92 \pm 0.55\,\mathrm{cpd/100\,t}$ [4] [25] due to its degeneracy with the ^{210}Bi spectrum which complicates its determination (due to the uncertainty in the concentration of the former and the feebleness of the latter), while the contribution from ^{8}B νs has been fixed to the HZ-metallicity rate $0.46\,\mathrm{cpd/100\,t}$ due to its small contribution in the energy range of interest.

- (^{7}Be ν's) The ^{7}Be solar ν flux presents two monoenergetic lines at 384 keV (B.R. $\sim$ 10%) and 862 keV (B.R. $\sim$ 90%). The corresponding rate for the 862 keV line is $46.3 \pm 1.1^{+0.4}_{-0.7}\,\mathrm{cpd/100\,t}$ with a total uncertainty of 2.7%.
- (pp ν's) The pp interaction rate is $134 \pm 10^{+6}_{-10}\,\mathrm{cpd/100\,t}$.
- (pep ν's) In order to extract the pep ν flux we constrained the CNO ν flux. With the current sensitivity the ^{7}Be and pp ν interaction rates are not affected by the ν's HZ vs ν's LZ hypothesis on CNO. However, the pep ν interaction rate depends on it, being $0.22\,\mathrm{cpd/100\,t}$ higher in the case of LZ hypothesis. In both cases the absence of pep reaction in the Sun is rejected at more than $5\,\sigma$.
- (CNO ν's) The e^- recoil spectrum induced by CNO ν's and the ^{210}Bi beta spectrum are degenerate. For this reason it is impossible to disentangle the two contributions with the spectral fit and only an upper limit on the CNO neutrinos contribution can be obtained. To indirectly constraint the pep ν's contribution we exploit the theoretically well known pp and pep flux ratio at a value of $R(\mathrm{pp/pep}) = (47.8 \pm 0.8)$ considering the HZ case[4] [4] [25] obtaining an upper limit on CNO ν rate of $8.1\,\mathrm{cpd/100\,t}$ (95 % C.L.).

In Table 2, the solar neutrino Borexino rate results and the correspondence to non-oscillated fluxes are summarized.

[4] Constraining R(pp/pep) to the LZ hypothesis value of 47.5 ± 0.8 gives identical results.

Table 2. Borexino results on solar neutrinos. In the third column the non-oscillated fluxes assume the MSW-LMA oscillation parameters [25]. The result on *pep* νs depends on whether we assume HZ or LZ metallicity for constraining CNO. Table adapted from [22].

Solar ν	Rate (cpt/100 t)	Flux ($cm^{-2}s^{-1}$)
pp	$134 \pm 10^{+6}_{-10}$	$(6.1 \pm 0.5^{+0.3}_{-0.5}) \cdot 10^{10}$
^7Be	$48.3 \pm 1.1^{+0.4}_{-0.7}$	$(4.99 \pm 0.11^{+0.06}_{-0.08}) \cdot 10^9$
$pep(HZ)$	$2.43 \pm 0.36^{+0.15}_{-0.22}$	$(1.27 \pm 0.19^{+0.08}_{-0.12}) \cdot 10^8$
$pep(LZ)$	$2.65 \pm 0.36^{+0.15}_{-0.24}$	$(1.39 \pm 0.19^{+0.08}_{-0.13}) \cdot 10^8$
^8B	$0.223^{+0.015+0.006}_{-0.016-0.006}$	$(2.57^{+0.17+0.07}_{-0.19-0.07}) \cdot 10^6$
CNO	$< 8.1 (95\% C.L.)$	$< 7.9 \cdot 10^8 (95\% C.L.)$

8. Improved measurement of ^{8}B solar neutrinos with 1.5 kt·y exposure

For the measurement of ^{8}B neutrinos we perform a complementary analysis, using the same analysis framework but setting the energy threshold at 3.2 MeV electron energy (i.e. 1650 p.e.)[5]. The dataset is wider compared to the one employed for the previous analysis of *pp*, ^{7}Be, and *pep* neutrinos; data have been collected from January 2008 to December 2016 corresponding to 2062.4 live days of data, omitting data during detector operations such as scintillator purification and calibrations.

The dataset has been split into two energy regions: a low energy range (LE), from 1650 to 2950 p.e., including events from natural radioactivity, and a high energy range (HE), from 2950 to 8500 p.e.. This high energy region is dominated by external γ-rays from neutron capture processes on the Stainless Steal Sphere.

Whilst HE sample use data from the whole active volume, the LE sample requires a spatial cut in order to remove the top layer of scintillator because of the presence of PPO solute from a scintillator leak in the upper buffer fluid volume caused by a small tear in the Inner Vessel present since early in Borexino's Phase I.

The total exposure is 1519 tonnes·years, and the time-averaged mass is 266.0±5.3 ton[6]. The mass fraction, for the LE sample after the z-cut at 2.5 m, is 0.857±0.006.

The HE data sample is fitted employing two components; the ^{8}B neutrinos and the external component from neutron captures. The LE sample requires three additional fit components, all due to ^{208}Tl isotope that is present in the bulk dissolved in the scintillator, at the surface of the nylon vessel, and from emanation diffused from the nylon vessel into the outer edge of liquid scintillator.

- (^{8}B ν's) The counting rate for the ^{8}B is $0.223^{+0.015+0.006}_{-0.016-0.006}$ cpd/100 t that is in good agreement with that expected from the HZ-SSM. See Table 2.

9. Measurement of the ratio $\mathcal{R}$ between the rates of ^{3}He-^{4}He and ^{3}He-^{3}He

It is possible to measure experimentally the ratio $\mathcal{R}$ between the rates of the ^{3}He-^{4}He and the ^{3}He-^{3}He reactions occurring within the *pp* chain, from the *pp* and ^{7}Be ν fluxes. [26]. This value represents the competition between the two primary modes of terminating the *pp* chain (encompassing all solar neutrino-producing reactions except CNO) and represents a robust probe into the solar fusion processes. Neglecting the *pep* and ^{8}B neutrino contributions, $\mathcal{R}$ can be written as:

[5] 500 p.e. correspond to about 1 MeV.

[6] Assuming a scintillator density of 0.8802 g/cm^3.

$$\mathcal{R} = \frac{2 \cdot \Phi(^7Be)}{\Phi(pp) - \Phi(^7Be)} \tag{3}$$

The measured value by Borexino is $\mathcal{R} = 0.178\,^{+0,027}_{-0,023}$ which is in agreement with the predicted values of the SSM for $\mathcal{R} = 0.180 \pm 0.011$ (HZ) and 0.161 ± 0.010 (LZ) [4].

10. Electron neutrino survival probability P_{ee}

Figure 6 shows the electron neutrino survival probability as function of the neutrino energy. The value for flavor conversion parameters from the MSW-LMA solution are taken from [27] Δm^2_{12}=7.50×10^{-5} eV^2, tan$^2\theta_{12}$=0.441, and tan$^2\theta_{13}$=0.022 (pink distribution in figure). In gray is reported the case of only vacuum LMA oscillations. For the ^{8}B neutrino flux both the HZ-B16 (GS98) SSM and the LZ-B16 (AGSS09met) SSM are assumed [4] [28] [7]. Dots represent the Borexino results for *pp* (red), ^{7}Be (blue) and *pep* (azure). ^{8}B neutrino measurements are in green for the LE+HE range, and grey for the separate sub-ranges. For the non-monoenergetic *pp* and ^{8}B neutrinos, dots are set at the mean energy of detected neutrinos and weighted on the detection range in electron recoil energy. The error bars include both experimental and theoretical uncertainties. The Borexino results are in agreement with the expectation of the MSW-LMA solution and for the first time they are obtained in a single experiment.

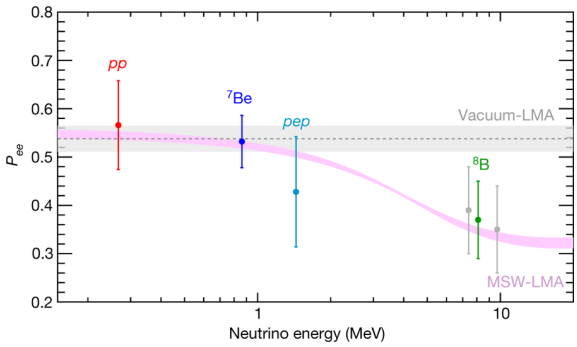

Figure 6. Electron neutrino survival probability as function of the neutrino energy.

11. Metallicity with ^{7}Be and ^{8}B ν fluxes

As we stated in section 2 a possible way to disentangle the LZ-SSM from the HZ-SSM is to measure the ^{7}Be, ^{8}B or *CNO* ν fluxes. The difference between these ν fluxes in the case of the two metallicities is about 9% for ^{7}Be ν_e, about 18% for ^{8}B ν_e. Thanks to Borexino measurements on ^{7}Be and ^{8}B ν_e it is possible to infer a first hint toward the metallicity issue.

Defining the reduced fluxes $f_{\rm Be} = \Phi(^7{\rm Be})/\Phi(^7{\rm Be})_{\rm HZ}$ and $f_{\rm B} = \Phi(^8{\rm B})/\Phi(^8{\rm B})_{\rm HZ}$ we can combine the new Borexino results on ν interaction rates and obtain the regions of allowed values. In Figure 7 the allowed contours, together with the 1σ theoretical predictions for LM and HM SSM, are shown. It seems that, even if not statistically significant, there is a weak hint in favor of the HZ SSM hypothesis. The discrimination between the LZ and HZ SSM is largely dominated by the uncertainties in the theoretical models.

12. Toward the CNO ν's measurement

Measuring CNO νs is paramount not only to directly probe the solar metallicity but also, and in particular, because so far the CNO cycle has never been directly experimentally measured.

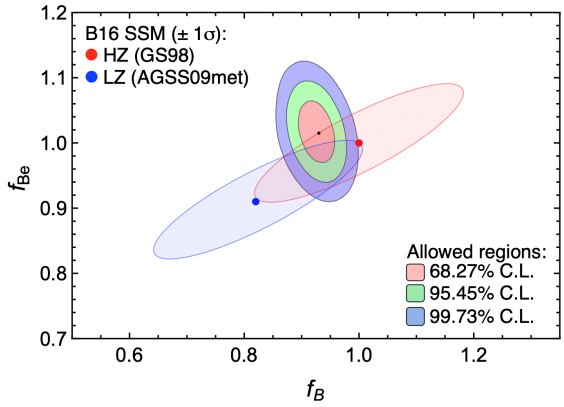

Figure 7. Allowed contours in the f_{Be}-f_{B} parameter space (see text).

According to the SSM, in the case of HZ and LZ predictions, we expect 4.91 ± 0.52 cpd/100t and 3.52 ± 0.37 cpd/100t respectively, to be compared with the current Borexino limit <8.1 cpd/100t (95% C.L.).

The most troublesome problem for the CNO ν measurement in Borexino is due to the β spectrum from ^{210}Bi within the ^{238}U chain, which is very similar to the elastic scattering signal from CNO νs. Indeed, the ^{210}Bi β spectrum is quasi-degenerate with the one coming from electrons recoiling off from CNO neutrinos. ^{210}Bi is a decay product of ^{222}Rn, and because of this is found in air and practically on all surfaces. It is sustained by its long-lived daughter ^{210}Pb, and is followed by the long-lived α emitter, ^{210}Po. To measure the CNO ν signal one could determine the ^{210}Bi activity by measuring the supported ^{210}Po component after the fraction which is out of equilibrium has decayed. Fortunately, thanks to the α/β discrimination techniques it is quite easy to identify the α particle from ^{210}Po – but a precise determination of the steady-state component is made difficult by background fluctuations caused by scintillator mixing due to convective motions induced by ambient temperature fluctuations. Starting from 2015 the Borexino detector has been thermally insulated from the environmental air of the experimental hall and it is hoped that with this stabler detector, ^{210}Bi will become low and constrained enough to allow for a measurement of CNO neutrinos in the very near future.

References

[1] Fowler, W.A. (1958) *Astrophys. J.*, *127*, 551–556.
[2] Cameron, A.W.G. (1958) *Annu. Rev. Nucl. Sci.*, *8*, 299–326.
[3] Bahcall, J.N.; Pinsonneault, M.H. (2004) *Phys. Rev. Lett.* , *92*, 121301.
[4] Vinyoles, N.; Serenelli, A.M.; Villante, F.L.; Basu, S.; Bergström, J.; Gonzalez-Garcia, M.C.; Maltoni, M.; Peña-Garay, C.; Song, N. (2017) *Astrophys. J.*, *835*, 202.
[5] Grevesse, N.; Sauval, A.J. (1998) . *Space Sci. Rev.*, *85*, 161–174.
[6] Asplund, M.; Grevesse, N.; Sauval, J. Special Isseu on Nuclear Astrophysics. (2006) *Nucl. Phys. A*, *777*, 1–702.
[7] Asplund, M.; Grevesse, N.; Sauval, A.J.; Scott, P. (2009) *Ann. Rev. Astron. Astrophys.*, *47*, 481–522.
[8] Serenelli, A.; Basu, S.; Ferguson, J.W.; Asplund, M. (2009) *Astrophys. J.*, 705
[9] S. Vagnozzi, K. Freese and T. H. Zurbuchen, (2017) *Astrophys. J.*, 839 55.
[10] S. Vagnozzi (2019) *Atom*, 7 41.
[11] V. Antonelli, L. Miramonti, C. Pea Garay, and A. Serenelli (2013) *Advances in High Energy Physics*, *ID* 351926.
[12] R. Davis, Nobel Prize Lecture. (2002)
[13] K.S. Hirata et al., (1999) *Phys. Rev. Lett. 63*, 16.
[14] Y. Fukuda et al., (1998) *Phys. Rev. Lett. 81*, 1562.
[15] W. Hampel et al., (1999) *Phys. Lett. B 447*, 127.
[16] M. Altmann et al., (2005) *Phys. Lett. B 616*,174.

[17] J.N. Abdurashitov et al., (1999) *Phys. Rev. Lett. 83*, 4686.
[18] B. Aharmim et al., (2007) *Phys. Rev. C 7*, 045502.
[19] Alimonti G., et al. (2009) *NIM A 600*, 568.
[20] Alimonti G., et al. (2009) *NIM A 609*, 58.
[21] Miramonti L., (2015) *Astr. Notes 336*, 790 doi.org/10.1002/asna.201512229.
[22] Borexino Collaboration (2018) *Nature 562*, 505
[23] G. Bellini *et al.* (2012) *Physical Review Letters 108*, 051302
[24] G. Bellini *et al.* (2014) *Physical Review D 89*, 112007
[25] I. Esteban *et al.* (2017) *Journal of High Energy Physics 01*,
[26] C. Peña-Garay, (2003) *Journal of High Energy Physics 11*
[27] I. Esteban, M. C. Gonzalez-Garcia, M. Maltoni, I. Martinez-Soler, and T. Schwetz, (2017) *JHEP 01*, 087
[28] N. Grevesse and A. Sauval, (1998) *Space Science Reviews* 85, *161.*